Persistent Ocean Monitoring with Underwater Gliders: Towards Accurate Reconstruction of Dynamic Ocean Processes

Ryan N. Smith, Mac Schwager, Stephen L. Smith, Daniela Rus and Gaurav S. Sukhatme

Abstract— This paper proposes a path planning algorithm and a velocity control algorithm for underwater gliders to persistently monitor a patch of ocean. The algorithms address a pressing need among ocean scientists to collect high-value data for studying ocean events of scientific and environmental interest, such as the occurrence of harmful algal blooms. The path planner optimizes a cost function that blends two competing factors: it maximizes the information value of the path, while minimizing the deviation from the path due to ocean currents. The speed control algorithm then optimizes the speed along the planned path so that higher resolution samples are collected in areas of higher information value. The resulting paths are closed circuits that can be repeatedly traversed to collect long term ocean data in dynamic environments. The algorithms were tested during sea trials on an underwater glider operating off the coast of southern California over the course of several weeks. The results show significant improvements in data resolution and path reliability compared to a sampling path that is typically used in the region.

I. INTRODUCTION

Path planning for Autonomous Underwater Vehicles (AUVs) is required for a wide variety of applications, such as mine countermeasures, ecosystem monitoring, locating hydrothermal vents, and tracking dynamic features. The algorithms presented here address the common problem in ocean science of designing a sampling method to acquire data at multiple spatiotemporal resolutions to analyze ocean processes. We consider a mission domain that contains user-specified regions of high interest. Our goal is to generate a long time-series data set for the mission domain, while providing finer sampling resolution in regions of high-interest.

To this end, the contributions of this paper are threefold. First, we develop a path planner to compute a single, repeatable path that is to be continually traversed by an AUV to generate a long time-series data set. The path is optimized for visiting regions of high interest, penalized for navigating through waters of large magnitude ocean currents, and is length constrained. Secondly, we develop a velocity control algorithm for autonomous gliders that varies the sampling resolution of the vehicle along each segment of

R. N. Smith is with the School of Engineering Systems at the Queensland University of Technology, Brisbane, QLD, 4000 Australia. ryan.smith@qut.edu.au

M. Schwager is with the GRASP Lab, University of Pennsylvania, Philadelphia, PA 19104, USA. schwager@seas.upenn.edu

S. L. Smith and D. Rus are with the Distributed Robotics Lab, Computer Science and Artificial Intelligence Laboratory, Massachusetts Institute of Technology, Cambridge, MA 02139, USA. slsmith@mit.edu, rus@csail.mit.edu

G. Sukhatme is with the Robotic Embedded Systems Laboratory, Department of Computer Science, University of Southern California, Los Angeles, CA 90089, USA. gaurav@usc.edu

a prescribed path. The velocity control directly corresponds to controlling the dive and ascent pitch angle of the glider during mission execution. Third, we validate our algorithms by implementing the optimized sampling strategy on vehicles in the ocean. This sea-trial demonstrates the ability of the method to perform a persistent monitoring application for resolving large-scale events, while simultaneously collecting high-resolution data for smaller-scale processes.

We apply the algorithms in this paper to study dynamic ocean events specifically arising in the Southern California Bight (SCB)[1] with a motivation to understand small-scale physical triggers for large scale events. The large-scale events of interest are algal and phytoplankton blooms; especially those composed of toxin producing species, commonly referred to as Harmful Algal Blooms (HABs). The environmental triggers leading to the onset, evolution and ultimate mortality of HAB events are currently widely unknown. Since coastal regions have high ecological and socio-economic importance [1], it is of interest to accurately assess, and predict such events and understand their impacts upon this fragile ecosystem.

Coastal ocean processes in southern California are driven primarily by large-scale (regional and global) processes, rather than local forcing, e.g., local winds. The dynamics are affected by multiple variables that oscillate over many different spatiotemporal scales that cannot be resolved by use of a few stationary sensors or via a single, short-term AUV deployment. A significant, long-term time-series of data are required to understand large-scale variability in this complex coastal ecosystem. Alternatively, smaller-scale processes significantly impact the biological dynamics in the SCB. Examples include the propagation of internal waves, sewage outfalls and river runoff into the ocean. Both events inject nutrient-rich water to the euphotic zone, and provide surplus food to photosynthetic organisms. Thus, in certain known areas, it is advantageous to collect higher resolution data. We may know where these *high-interest* regions are, but either from lack of historical data or data at the appropriate resolution, we still do not fully understand the biophysical dynamics occurring in them. The algorithms proposed here address the need for continual sampling at variable resolutions by providing high-resolution data in areas of known importance.

Although there is a formidable literature on planning information rich paths for environmental monitoring, most

---

[1]The SCB is the oceanic region contained within $32°$ N to $34.5°$ N and $-117°$ E to $-121°$ E.

existing techniques are not well suited to the unique constraints and capabilities of underwater gliders. One existing method is to plan covering paths over the environment. Examples of this appear in agriculture [2], [3], general robotics [4], and AUV applications [5]. These methods rely on a finite sensor footprint whereas the typical suite of ocean sensors take only point measurements. Other approaches to surveillance and monitoring with AUVs essentially boil down to achieving the best estimation or re-creation of a scalar field via intelligent planning or adaptive sampling [6], [7], [8]. These methods are not well suited to the piece-wise linear paths along which underwater vehicles must travel. Finally, there has recently been work on persistent monitoring [9], [10], where the frequency of visits to each region is adapted to the time scale on which that region changes. This study is directed towards developing a sampling strategy that is sensitive to the information value of different regions, while being naturally amenable to the unique constraints of the underwater glider.

We organize the rest of this paper in the following way. We begin with a short description of the AUV and ocean model used in this research in Section II. Section III gives a detailed problem description. Section IV presents a path planning algorithm for long-term AUV data collection. Section V defines an algorithm to vary the sampling resolution along the path generated in Section IV. We present experimental results and analysis of sea trials to validate our methods in Section VI. We finish this study with some concluding remarks and areas of future investigation and extensions.

II. AUTONOMOUS UNDERWATER VEHICLE AND OCEAN MODEL

The vehicle used in this study is a Webb Slocum autonomous underwater glider [11], see Fig. 1(a). A Slocum glider is a 1.5 m (length) by 21.3 cm (diameter), torpedo-shaped vehicle designed for long-term ($\sim$ 1 month) ocean sampling and monitoring [12], [13]. These gliders *fly* through the water by altering the position of their center of mass and changing their buoyancy. The glider navigates between predetermined waypoints with a sequence of dives and climbs forming a vertical sawtooth pattern; an optimal way to generate high-resolution spatial and temporal data with minimal energy expense. Due to this method of locomotion, gliders are slow moving AUVs and have operational velocities on the same order of magnitude as oceanic currents ($\backsim$ 0.75 km/hr). Between pre-programmed surfacings for GPS fixes and data transfer, the glider dead reckons its position using a magnetic compass, depth sensor, and altimeter. For specific operational details of Slocum gliders, see e.g., [11] or [12]. Based on considerable previous work on modeling and control of underwater gliders, [14], [15], we do not address this here. However, due to the complexity of the underwater environment, we aim to minimize adverse effects from ocean currents by utilizing ocean model predictions. The ocean model predictions used here come from the Regional Ocean Model System (ROMS) run at the Jet Propulsion Laboratory, California Institute of Technology. This model is a split-explicit, free-surface, topography-following-coordinate
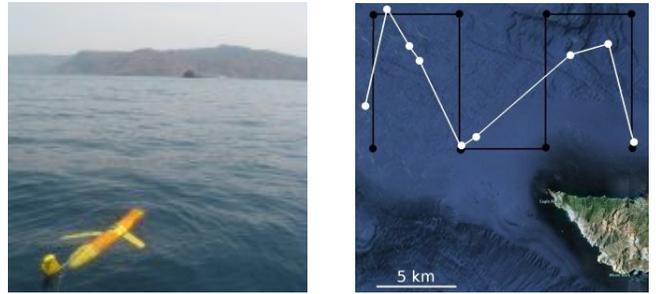
(a) Slocum glider.   (b) Lawnmower experiment.

Fig. 1. (a) One of the two Slocum gliders owned and operated by the USC CINAPS [16]. The glider is preparing to start a mission just off the Northeast coast of Santa Catalina Island, CA. (b) Planned lawnmower pattern (black waypoints and path) and the actual executed path (white surfacing locations and path) from a glider deployment off of the north coast of Santa Catalina Island, CA.

oceanic model that is open-source and widely accepted and supported throughout the oceanographic and modeling communities. Detailed information on ROMS can be found in [17] and [18]. ROMS provides hindcasts, nowcasts and hourly forecasts (up to 72 hours) for the SCB, [19], [20]. The model outputs have nested horizontal resolutions, covering the U.S. west coastal ocean (15 km), the southern California coastal ocean (5 km) and the SCB (2.2 km). We denote the set of points in the 2.2 km resolution grid as H.

III. PROBLEM DESCRIPTION

We compute a single, repeatable path that is continually traversed by the vehicle to generate a long time-series data set. Along this path, we optimize the velocity of the vehicle to alter the spatiotemporal sampling resolution throughout a region of interest. Repeated traversal of a regular path allows for easier assimilation of collected data with existing data or measurements, as well as has the added incentive that known obstacles (e.g., shipping lanes, sea mounts, harbor entrances, etc.) can be avoided and planned for *a priori*. Through this technique, we aim to gather data relating to large-scale events, e.g., algal blooms, while also resolving smaller-scale features, e.g., internal wave structures, that influence and drive the mechanistic processes of the larger scale phenomena. For such a survey, the common choice is a lawnmower-type path. For implementations onto autonomous gliders, an *optimized* lawnmower-type path may not be the best choice. In particular, Fig. 1(b) displays a planned lawnmower path in black, and the actual executed path by a glider in white. Notice the zig-zag structure of the executed path in the attempt to realize the prescribed lawnmower pattern. Such experimental results motivate us to consider a zig-zag-shaped path that broadly covers the region of interest, passes through specified *high-interest* areas, and minimizes the effects of strong ocean currents. This method generates a regular, repeatable path that can be used for persistent monitoring efforts to collect data that facilitates analysis of phenomena at multiple spatiotemporal scales.

In order to formally describe our problem, we require some notation. We consider a mission domain $Q \subset \mathbb{R}^2$.
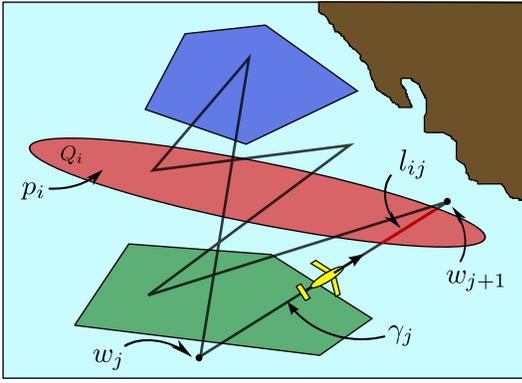
Fig. 2. A schematic example of a computed glider path. The viewable region represents Q. The regions of interest Q_i are colored based on their user-defined importance p_i. The intersection of region Q_i with segment γ_j is given by l_{ij}. The proposed optimization algorithm in Section V produces a set of pitch angles ϕ_j for the glider to implement along each segment γ_j to achieve an appropriate sampling resolution.

Fig. 3. A general overview of the experimental area off the coast of southern California. The mission domain Q is delineated by the white polygon. Regions Q_1, Q_2 and Q_3 are the high interest regions, and are delineated by the red, green and yellow polygons, respectively. The grey shaded polygons denote the checkerboard regions, and the yellow regions to the west of the mission domain are the primary shipping lanes for Long Beach Harbor.

Within Q there are $n - 1$ regions of interest $Q_i \subset Q$, where $i \in \{1, \ldots, n-1\}$. We define an nth region $Q_n = Q \setminus \cup_{i=1}^{n-1} Q_i$ to be the *background*. Thus, we have $Q = \cup_{i=1}^{n} Q_i$. Each region Q_i, $i \in \{1, \ldots, n\}$ is assigned an importance level $p_i \in [0, 1]$. We assume that the regions $Q_1, \ldots, Q_{n-1}$ are specified by an ocean scientist, and the weights p_i determine the relative sampling importance of a region with respect to all other regions. Through these user-defined regions, we aim to encode certain oceanographic information, such as preferred sampling direction and appropriate horizontal and vertical scaling. Our goal is to compute a closed-path γ consisting of $0 < m < \infty$ waypoints that steer the vehicle through the regions Q_i, $i \in \{1, \ldots, n-1\}$ while avoiding areas of predicted, high-magnitude ocean currents. This notation is presented graphically in Fig. 2.

Dealing with repeatability and minimizing uncertainty along a path are complex issues when considering an underwater vehicle. The ocean is a highly dynamic, time-varying, nonlinear system that imparts large magnitude external forces upon the vehicle. Some of these forces and moments, like buoyancy and viscous damping, can be estimated with reasonable accuracy for a given vehicle, e.g., see [21]. However, the forces and moments related to ocean currents can greatly affect the navigational accuracy of a dead reckoning glider [22], [23]. In this study, consideration of ocean currents is based on ROMS predictions. We consider historical ROMS predictions for 30 days prior to the deployment. For each daily prediction, we consider 24 hours of the forecast. At each grid point in H, we find the maximum magnitude of the ocean current between 0 and 80 m depth. Since strong currents in any direction effect the glider's navigational accuracy, we only consider magnitude, and do not take current direction into account at this phase of the study. The magnitudes at each location for each day are then averaged over the 30-day time window. By interpolating between the grid points in H, we create a function $\nu : Q \mapsto \mathbb{R}_{\geq 0}$, which gives the average maximum magnitude current expected at each point in Q. We remark that the grid points of H are at least as fine as the observed surfacing error of the glider.

In the following sections we present two decoupled algorithms that design a sampling strategy for persistent and adaptive monitoring of an oceanic region with designated areas of *high-interest*. The path planner presented in Section IV details an optimization that rewards visiting each Q_i and penalizes navigation through areas of typically large magnitude ocean currents. The algorithm presented in Section V optimizes the velocity along each segment of a sampling path to obtain an adaptive sampling resolution for each Q_i, while maintaining an overall time budget for the traversal of γ.

IV. PATH PLANNING

The path planning algorithm requires the following inputs: 1) the mission domain Q; 2) the high interest regions Q_i, with associated weights p_i, $i \in \{1, \ldots, n\}$; 3) the desired number of waypoints $m < \infty$; and 4) a line L dividing Q into two halves, and defining the ordinate axis of the proposed zig-zag path. Given m, let $\{w_1, \ldots, w_m\}$ be the m waypoints that define the path γ, and for each $j \in \{1, \ldots, m\}$, let γ_j be the line segment connecting the endpoints w_j and w_{j+1}, where we let $w_{m+1} := w_1$. Then, given L, this algorithm generates an alternating *checkerboard* pattern; the grey regions shown in Fig. 3. The path is created by choosing one waypoint in each square of the checkerboard, such that it minimizes a cost function capturing both a penalty for high ocean currents and a reward for traversing through high-interest regions.

Let waypoint w_j lie in checkerboard square j. We evaluate the effect of ocean currents as follows. Given $\nu : Q \to \mathbb{R}_{\geq 0}$, the cost of a path due to ocean currents is given by

$$\sum_{j=1}^{m} \int_{\gamma_j} \nu(q)dq,$$

where the velocity of a point $q \notin H$ is given by the velocity of its nearest neighbor in H.

The reward for passing through regions Q_i is defined as follows. Define the length of the intersection of a region Q_i with a path segment γ_j by $l_{ij} = |Q_i \cap \gamma_j|$, where $|\cdot|$ denotes the length of the segment. For a given path γ, the length of γ passing through region Q_i is $\sum_{j=1}^{m} l_{ij}$. Since we want to spend more time in regions of higher interest, we define the benefit as

$$\sum_{i=1}^{n} p_i \sum_{j=1}^{m} l_{ij}.$$

Therefore, the cost of a set of waypoints $W = \{w_1, \ldots, w_m\}$ is defined as

$$H(W, \lambda) := \lambda \sum_{j=1}^{m} \int_{\gamma_j} \nu(q) dq - (1 - \lambda) \sum_{i=1}^{n} p_i \sum_{j=1}^{m} l_{ij},$$

where $\lambda \in [0, 1]$. Here, λ acts primarily as a scaling factor to equivocate the magnitude of the different units in the considered cost functions. For small λ, we compute longer distance paths, while for $\lambda \approx 1$ we generate shorter paths. Given $\lambda \in [0, 1]$, we search all possible sets of m waypoints for the set W^* that minimizes $H(W, \lambda)$.

First, we compute $Q \cap H$ to discretize Q, so that each checkerboard region contains a finite number of candidate waypoints. Then, define a graph whose vertices are these discretized points, and whose edges connect waypoints in checkerboard square j to waypoints in square $j + 1$. The weight on an edge connecting w_j to w_{j+1} is given by

$$\lambda \int_{\gamma_j} \nu(q) dq - (1 - \lambda) \sum_{i=1}^{n} p_i l_{ij}.$$

This defines a directed graph, where every cycle is of the form $w_1, \ldots, w_m, w_1$. Thus, by fixing w_1, we can find the shortest cycle returning to w_1 by use of the Bellman-Ford algorithm. Minimizing repeated applications of Bellman-Ford algorithm for each candidate waypoint w_1 determines the set W^* that minimizes $H(W, \lambda)$. The above description is summarized in Alg. 1. Given a graph containing N vertices, Bellman-Ford algorithm runs in $O(N^3)$ time. Thus, the ZZTOPP algorithm runs in $O(N_1 N^3)$ time where N is the number of points in the disretization, and N_1 is the number of points in checkerboard square $j = 1$.

By use of Alg. 1 we plan a sampling path to study algal bloom life-cycles within the SCB. For a detailed presentation of this ongoing study, please see [16]. We choose $m = 6$. In Fig. 3 the region of interest Q is given by the white polygon, L is the black line through Q, the yellow lines denote the primary shipping lanes to be avoided, high-interest regions Q_1, Q_2 and Q_3 are denoted by the red, green and yellow polygons within Q, respectively, and the six computed checkerboard regions are given by the grey regions. Algal blooms have an episodic time of ~ 10 days, thus, one cycle of γ must be traversable in < 5 days[2]. This corresponds to a total path length of less than 110 km. The other inputs to ZZTOPP for the path optimization are: $\lambda = 0.4$, $p_1 = 1$,

---

[2]Standard Nyquist sampling theory states that the sampling frequency must be at least one half the epoch of the event under study to adequately resolve the variability.

Algorithm 1: Zig-Zag in the Tranquil Ocean Path Planner (ZZTOPP)

Input : 1) The high interest regions Q_i and their associated importance levels p_i; 2) the number of waypoints m; 3) the axis L; and 4) the parameter $\lambda \in [0, 1]$.

Output: A set W of m waypoints minimizing the cost function $H(W, \lambda)$.

1 Compute the checkerboard regions from the line L and number of waypoints m.

2 Determine average magnitudes for ocean current velocities from ROMS data $\nu : Q \to \mathbb{R}_{\geq 0}$.

3 Discretize checkerboard regions.

4 Generate a graph G with vertices given by discretized points, edges connecting each point in checkerboard region j to each point in checkerboard region $j + 1$.

5 Compute edge weights. For edge connecting w_j and w_{j+1}, the weight is

$$\lambda \int_{\gamma_j} \nu(q) dq - (1 - \lambda) \sum_{i=1}^{n} p_i l_{ij}.$$

6 foreach candidate waypoint w_1 **do**

7   Compute shortest cycle in G containing w_1 using Bellman-Ford algorithm.

8   Store waypoints on minimum cost cycle as W.

9 Output W.

$p_2 = 0.75$, $p_3 = 0.7$, the background importance $p_n = 0.3$, and the location of checkerboard region $j = 1$ is the northeast corner of Q.

For this experiment, we had to extend checkerboard region $j = 5$ to include the area within Q_2, see Fig. 4. Based on the location of Q_2 and checkerboard region $j = 1$, odd m is operationally unsafe, as the path from w_m to w_1 could cross over land. For m even, the intersection of Q_2 and checkerboard region $m - 1$ was not a large enough area to guarantee a minimal path through Q_2. Addressing this issue is an area of future work.

Applying the ZZTOPP Algorithm with the given inputs produces the black path in Fig. 4. We will hereafter refer to this path as the *computed* path. The magenta path in Fig. 4 is a path that was hand-designed by an ocean scientist for the same application presented here. We will hereafter refer to this path as the *reference* path.

V. SAMPLE RESOLUTION OPTIMIZATION

We now present an algorithm to assign different sampling resolutions to different regions in a mission domain based on the relative importance of those regions. The sampling resolution for a glider is altered by changing the pitch angle of the saw tooth pattern that the glider executes as it traverses the segments of the given path.

The behavior of a glider on segment γ_j, $j \in \{1, \ldots, m\}$ is controlled by the following quantities:
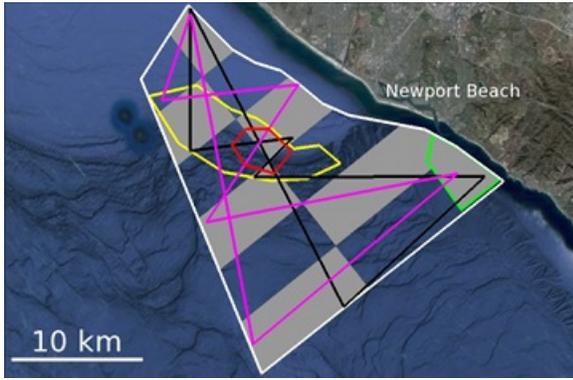
Fig. 4. This figure presents an enlarged view of Figure 3 with the glider paths overlaid. The path produced by the ZZTOPP Algorithm is given by the black line, while the magenta line represents the reference path that was hand-delineated by an oceanographer to survey the same region with the same constraints. The mission domain Q is delineated by the white polygon. Regions Q_1, Q_2 and Q_3 are the high interest regions, and are delineated by the red, green and yellow polygons, respectively. The grey shaded polygons denote the checkerboard regions.
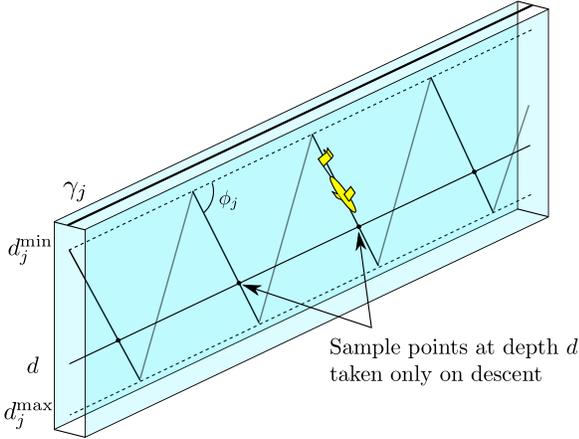
Fig. 5. The sawtooth pattern that the glider follows along each path segment γ_j is shown with its relevant parameters labeled. The sawtooth pitch ϕ_j controls the sample density, which we define as the number of samples per distance at a fixed depth d.

1) pitch angle $\phi_j \in [\phi_j^{\min}, \phi_j^{\max}]$
2) minimum depth $d_j^{\min}$, and
3) maximum depth $d_j^{\max}$.

Define the sample density in a region Q_i, denoted by ϱ_{Q_i}, to be the number of samples taken in region Q_i at a given depth, divided by total length of the path in Q_i. Similarly, we define the sample density along a segment γ_j, denoted by ϱ_{γ_j}, to be the number of samples at a given depth, divided by l_{ij}. Each time the glider descends along the edge of a tooth, it takes at most one sample at a given depth d, (to identify hysteresis effects, the glider does not take measurements while ascending), as shown in Fig. 5. The sample density ϱ_{γ_j} along segment γ_j, assuming an idealized triangular sawtooth (ignoring currents, disturbances, hydrodynamics

effects, etc.), is found from simple geometry to be

$$\varrho_{\gamma_j} = \frac{\tan \phi_j}{2(d_j^{\max} - d_j^{\min})}. \tag{1}$$

Then, we compute the sample density in a region Q_i as the number of samples in that region at a fixed depth, divided by the total length of the path in Q_i,

$$\varrho_{Q_i} = \frac{1}{L_i} \sum_{j=1}^{m} l_{ij} \varrho_{\gamma_j},$$

where $L_i := \sum_{j=1}^{m} l_{ij}$ is the total length of the path in Q_i.

We propose that the pitch angles $\phi_1, \ldots, \phi_m$ be set so as to maximize a measure of the total sampling benefit. The optimization of the pitch angles is subject to constraints on the minimum and maximum pitch, as well as on the total time to complete one cycle of the path. Now, consider a region Q_i and its sampling resolution ϱ_{Q_i}. Naturally, in increasing the sampling resolution ϱ_{Q_i}, we increase the "benefit." However, it is intuitive that this benefit will be subject to *diminishing returns*. This can be captured via a concave, monotonic function $H : \mathbb{R}_{\geq 0} \to \mathbb{R}_{\geq 0}$, satisfying $H(0) = 0$. In the experiments section $H(z) = \sqrt{z}$.

We define the total benefit of a set of pitch angles as

$$C(\phi_1, \ldots, \phi_m) := \sum_{i=1}^{n} p_i H(\varrho_{Q_i}). \tag{2}$$

Since H is concave, the benefit C is also concave. To compress notation, we define

$$\beta_{ij} = \frac{l_{ij}}{2L_i(d_j^{\max} - d_j^{\min})}, \quad \beta_i = [\beta_{i1} \ \cdots \ \beta_{im}]^T,$$
$$x_j = \tan \phi_j, \quad \text{and} \quad x = [x_1 \ \cdots \ x_m]^T,$$

so that $\varrho_{Q_i} = \beta_i^T x$. Also, define the vectors

$$x_j^{\min} = \tan \phi_j^{\min}, \quad x^{\min} = [x_1^{\min} \ \cdots \ x_m^{\min}]^T,$$
$$\text{and } x_j^{\max} = \tan \phi_j^{\max}, \quad x^{\max} = [x_1^{\max} \ \cdots \ x_m^{\max}]^T.$$

With the above definitions, the benefit in (2) is written as

$$C(x) = \sum_{i=1}^{n} p_i H(\beta_i^T x).$$

The final component of the optimization is the time constraint. We require that a complete cycle of the path be completed within a user specified time $T > 0$. Letting $v_{\text{hor},j}$ be the over-the-surface (or horizontal) speed of the glider along segment γ_j, the total time to complete the path is given by

$$\sum_{j=1}^{m} \frac{|\gamma_j|}{v_{\text{hor},j}}.$$

We have performed experiments to determine $v_{\text{hor},j}$ as a function of ϕ_j for the operating regime of pitch angles $15° \leq \phi_j \leq 35°$. By performing a least-squares fit, we obtain a relationship of

$$v_{\text{hor},j} = a x_j + b, \tag{3}$$

where $a := -0.05 \ m/s$, and $b := 0.275 \ m/s$. The coefficient of determination (or R^2 value) is 0.986 indicating a good linear fit.

Combining the above, the optimization of pitch angles can be written as

$$\text{maximize} \quad \sum_{i=1}^{n} p_i H(\beta_i^T x)$$
$$\text{subject to} \quad x^{\min} \le x \le x^{\max},$$
$$\sum_{j=1}^{m} \frac{|\gamma_j|}{ax_j + b} \le T,$$

where p_i is the importance level of region i; x is the optimization vector $x = [\tan \phi_1, \ldots, \tan \phi_m]$, with bounds $x^{\min} := \tan 15\,^\circ$ and $x^{\max} := \tan 35\,^\circ$; and $T > 0$ is the user-defined time budget.

The above optimization is convex. To see this, note that the objective function is concave. Thus we are maximizing a concave function (or equivalently, minimizing a convex function $-C(x)$). The constraints in $x^{\min} \le x \le x^{\max}$ form convex sets. Finally, since $x_j < b/a \approx 5.5$ for all $x_j \in [x^{\min}, x^{\max}]$, the denominator of the time constraint $ax_j + b$ is strictly positive, and the time constraint also yields a convex set. Therefore, the optimization can be efficiently solved using standard convex optimization tools [24]. In the following section we present experimental results in combining the path planning and speed optimization for adaptive ocean sampling.

VI. EXPERIMENTS

For demonstration and validation of the algorithms and their outputs presented in the previous sections, we provide data collected from sea trials. We deployed a Slocum glider in the SCB for one month for implementation of our computed missions. For this study, we considered two closed-loop sampling paths. Since the region of interest selected in this study is under active investigation by the USC CINAPS team [16], we choose one path to be the *reference* path; designed by an ocean scientist with extensive domain knowledge. This path has been traversed by Slocum gliders multiple times over the past two years, giving ample data for future comparison. In this study, the reference path was executed using the standard operating procedure; constant dive and ascent pitch angles of $26°$. We also applied the algorithm presented in Section V to the reference path, and computed an alternate implementation that varies the velocity of the vehicle by prescribing pitch angles ranging between $15°$ and $35°$[3]. The computed angles for each γ_j of this implementation are presented in Table I. The second path considered is one determined by an immediate predecessor of the ZZTOPP algorithm,[4] which gives a lower cost than

---

[3]The range of angles was chosen based on the operational constraints of the vehicle, and to minimize impacts on data collection and navigational accuracy.

[4]At the time of the experiments our algorithm used a suboptimal path planner, but with the same cost function $H(W, \lambda)$. The ZZTOPP planner presented here finds the globally optimal path with respect to this cost function.

the reference path, as shown in Table I. This computed path was executed with the pitch angles computed by use of the sampling resolution optimization algorithm given in Section V. The computed angles for each γ_j of this path are also presented in Table I.

The experimental results are divided into three parts to test separate portions of the algorithms. First, we will compare collected science data in a region of high interest for the minimum, standard and maximum dive and ascent angles, $15°$, $26°$ and $35°$, respectively. Secondly, we compare the traversibility of the two different paths, i.e., which path was followed more accurately by the glider. Lastly, we compare the total time of traversal for the three missions.

A. Variable Resolution

A goal of our work is to provide persistent monitoring of a given area with the added capability to adapt the sampling resolution to gather finer resolution data in areas of increased spatiotemporal variability. As previously mentioned, examining the area around the shelf region (Q_3 and Q_1) could lead to a better understanding of the environmental triggers that cause algal blooms. Recent analysis of glider data collected along γ_3 of the reference path has shown the possibility of resolving internal wave propagation. Internal waves are waves that arise from perturbations in hydrostatic equilibrium and oscillate within, rather than on the surface of, a fluid medium. In this case, the internal waves propagate on the interface between different densities of sea water, i.e., just below the thermocline. These waves break as the water depth decreases across the shelf, which promotes vertical mixing in the water column and may lead to the development of an algal bloom.

Based on experimental trials, a safe operational range for pitch angles for the glider was determined to be $15° - 35°$. To investigate the difference in sampling resolution, we executed cross-shelf transects through Q_1 at pitch angles of $15°, 26°$ and $35°$. The path for these transects is γ_3 of the reference path, for comparison at a later date with previously collected data. The temperature (°C) data collected during these experiments is presented in Figs. 6(a), 6(b) and 6(c). In these figures, we display the individual measurements taken by the vehicle to emphasize the difference in sampling resolution. These measurements are generally interpolated to a standard grid to create a continuous image of the water column. From the presentation here, it is clear that by increasing the pitch angle of the glider's dive and ascent, we are significantly altering the spatiotemporal resolution at which the data are gathered. This is most evident in deeper water, as the profiles in Fig. 6(a) are clearly spread apart, whereas those in Fig. 6(c) are much closer together. Also, there is a noticeable difference in resolution between the data collected at $26°$ (standard) versus $35°$.

As noticed in previous data collects, there is a distinct wave pattern propagating just below the thermocline. The internal waves seen in Figs. 6(a)-6(c) are propagating across the shelf and have a wavelength of ~ 2 km mid-shelf with a decrease in wavelength moving towards the shore. Such artifacts are difficult to resolve if only considering data
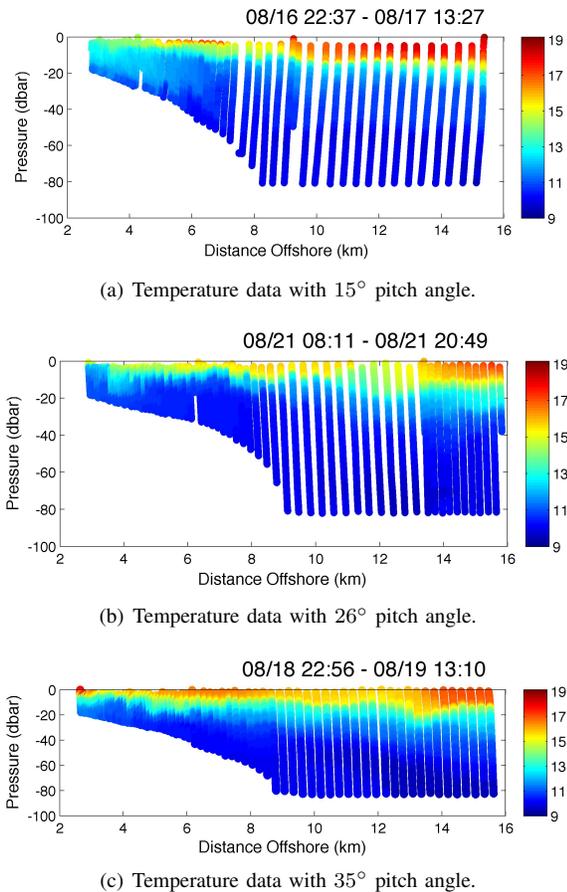
(a) Temperature data with 15° pitch angle.

(b) Temperature data with 26° pitch angle.

(c) Temperature data with 35° pitch angle.

Fig. 6. Pressure vs. Distance from Shore plots of Temperature (°C) data collected along the same transect for 6(a) 15°, 6(b) 26° and 6(c) 35°. Individual measurements are shown to emphasize the sampling resolution along each path. Start and end times for the transect are shown above each respective figure, with the year assumed to be 2010.

as in Fig. 6(a), or even in Fig. 6(b). However, with the increased sampling resolution provided with a pitch angle of 35° (Fig. 6(c)), smaller-scale and dynamic processes can be resolved more easily. In addition, since data from glider profiles are usually interpolated, one may wash out features that are of primary interest, e.g., shorter wavelength internal waves. These data provide an excellent motivation to continue the design of sampling missions to gather data at multiple spatiotemporal scales.

B. Navigational Accuracy

To assess the effectiveness of the ocean current consideration used in the ZZTOPP algorithm, we compare the navigational accuracy of the three implemented experiments. We compare the prescribed path with the executed path by use of the following metric. We delineate the glider's executed path by connecting sequential surfacing locations during the mission. We then compute the area between the executed path and the prescribed path. This essentially integrates the positional error along the entire closed-loop path. This area measure is used as the navigation score, with a smaller score indicating a more accurately navigated path.

	Reference Path (Standard)	Reference Path with Speed Control	Computed Path with Speed Control
Prescribed Path Length (km)	97.3	97.3	99.2
Pitch Angles $(\gamma_1, ..., \gamma_6)$	$(26°, 26°, 26°, 26°, 26°, 26°)$	$(15°, 27°, 35°, 35°, 25°, 15°)$	$(15°, 35°, 35°, 25°, 35°, 35°)$
Actual Distance Traveled (km)	93.51 ± 4.58	105	102
Total Traversal Time (hhh:mm)	$110:02 \pm 000:20$	$126:26$	$115:53$
Navigation Score (km^2)	70.35 ± 13.35	86.06	56.23
$H(W^*, \lambda)$	$-20,280$	$-20,280$	$-24,638$

For the reference path with the standard implementation, we average the results from ten recent loop traversals. Experimental results are presented in the first column of Table I, including one standard deviation uncertainties. For these ten standard executions of the reference path, we see an average navigation score of 70.35 km^2 with a standard deviation of 13.35 km^2. For the execution of the reference path with speed control, the navigation score increased to 86.06 km^2. For the path computed by use of the predecessor of the ZZTOPP algorithm, implemented with speed control, we get a navigation score of 56.23 km^2. This is significantly less than either type of execution of the reference path.

C. Loop Traversal Time

An important component of the path design is to assist in resolving the frequency of ocean phenomena occurring at different spatiotemporal resolutions. Thus, a computed path incorporating any variations in velocity must not be slower than the reference path with standard operational procedures. In Table I we present the total time of traversal for one loop of each of the three executed mission scenarios. For ten recent executions of the standard reference path, we see an average loop traversal time of 110.03 hours. This average lies well within the desired traversal time of $4 - 5$ days ($96 - 120$ hours), as mentioned previously. For the reference path executed with speed control, we have a loop traversal time of 126.43 hours. Although this time is greater than the 120 hours desired, it is not excessively long. The primary reason for the extra time required is the additional 9 km traveled during execution due to poor navigational accuracy. For the computed path executed with speed control, we see a loop traversal time of 115.88 hours. This is slightly longer than the reference path with standard execution, but still lies well within the desired time range.

VII. CONCLUSIONS AND FUTURE WORKS

We presented two algorithms that together produce paths for underwater gliders to provide persistent multi-scale resolution of dynamic ocean processes. First, we computed a closed path to be continually traversed by a vehicle. Then,

along this path we optimized the speed of the vehicle (by altering its pitch angle) to tune the spatiotemporal sampling resolution throughout the region of interest. We implemented our planned paths on autonomous gliders operating in a widely studied area off the coast of southern California. Data collected from the experiments were compared with historical data from a reference path. Theoretical predictions compared well with experimental results, as we saw that our path covered more distance in less time with better accuracy than previous implementations of the nominal path. The experimental results suggest that our algorithms provide the ability to perform long-term, persistent monitoring to capture large-scale event frequencies, while additionally resolving smaller-scale events by locally modifying spatiotemporal sampling resolution. Future field trials are required for further validation, but this preliminary analysis provides sufficient motivation for additional experiments.

For future study, one extension of this project is to combine the two algorithms presented in Sections IV and V to create a single path planning and speed optimization algorithm. Secondly, we are planning more sea trials to extensively test our computed paths and variation of the spatiotemporal sampling resolution. Finally, we will review the data collected in this work with an expert oceanographer with detailed domain knowledge to determine whether or not the sampling techniques presented here have provided *better* data with which to resolve internal waves and other small-scale events while also collecting data for large-scale processes.

VIII. ACKNOWLEDGMENTS

REFERENCES

[1] U.S. Commission on Ocean Policy, *An Ocean Blueprint for the 21st Century*. Washington, D.C., September 2004. ISBN#0-9759462-0-X, http://oceancommission.gov/.

[2] T. Oksanen, *Path Planning Algorithms for Agriculture Field Machines*. PhD thesis, Helsinki University of Technology, Espoo, Finland, December 2007.

[3] M. Taïx, P. Souéres, H. Frayssinet, and L. Cordesses, "Path planning for complete coverage with agricultural machines," in *Field and Service Robotics* (S. Yuta, H. Asama, E. Prassler, T. Tsubouchi, and S. Thrun, eds.), vol. 24 of *Springer Tracts in Advanced Robotics*, pp. 549–558, Springer Berlin / Heidelberg, 2006.

[4] H. Choset, "Coverage of known spaces: The boustrophedon cellular decomposition," *Autonomous Robots*, vol. 9, pp. 247 – 253, 2000.

[5] S. Anstee and C. Fang, "Coverage path planning for harbour surveys using an AUV," in *Proceedings of the IEEE Oceans Conference*, (Sydney, Australia), May 2010.

[6] A. Singh, A. Krause, C. Guestrin, and W. Kaiser, "Efficient informative sensing using multiple robots," *Journal of Artificial Intelligence Research*, vol. 34, pp. 707–755, 2009.

[7] D. Paley, F. Zhang, and N. Leonard, "Cooperative control for ocean sampling: The glider coordinated control system," *IEEE Transactions on Control Systems Technology*, vol. 16, pp. 735–744, July 2008.

[8] C. McGann, F. Py, K. Rajan, J. P. Ryan, and R. Henthorn, "Adaptive control for autonomous underwater vehicles," in *Proceedings of the Association for the Advancement of Artificial Intelligence*, (Chicago, IL), 2008.

[9] S. L. Smith and D. Rus, "Multi-robot monitoring in dynamic environments with guaranteed currency of observations," in *IEEE Conference on Decision and Control*, (Atlanta, GA), pp. 514–521, Dec. 2010.

[10] S. L. Smith, M. Schwager, and D. Rus, "Persistent robotic tasks: Monitoring and sweeping in changing environments," *IEEE Transactions on Robotics*, July 2010. Submitted.

[11] Webb Research Corporation. http://www.webbresearch.com/slocum.htm, 2008. viewed September 2010.

[12] O. Schofield, J. Kohut, D. Aragon, E. Creed, J. Graver, C. Haldman, J. Kerfoot, H. Roarty, C. Jones, D. Webb, and S. Glenn, "Slocum gliders: Robust and ready," *Journal of Field Robotics*, vol. 24, no. 6, pp. 473–485, 2007.

[13] G. Griffiths, C. Jones, J. Ferguson, and N. Bose, "Undersea gliders," *Feeding and Healing Humans*, vol. 2, no. 2, pp. 64–75, 2007.

[14] N. Leonard and J. Graver, "Model-based feedback control of autonomous underwater gliders," *IEEE Journal of Oceanic Engineering, Special Issue on Autonomous Ocean-Sampling Networks*, vol. 26, pp. 633–645, Oct. 2001.

[15] J. G. Graver, *Underwater Gliders: Dynamics, Control and Design*. PhD thesis, Princeton University, 2005.

[16] R. N. Smith, J. Das, H. Heidarsson, A. Pereira, I. Cetinić, L. Darjany, M. Ève Garneau, M. D. Howard, C. Oberg, M. Ragan, A. Schnetzer, E. Seubert, E. C. Smith, B. A. Stauffer, G. Toro-Farmer, D. A. Caron, B. H. Jones, and G. S. Sukhatme, "USC CINAPS builds bridges: Observing and monitoring the Southern California Bight," *IEEE Robotics and Automation Magazine, Special Issue on Marine Robotics Systems*, vol. 17, pp. 20–30, March 2010.

[17] A. F. Shchepetkin and J. C. McWilliams, "The regional oceanic modeling system (ROMS): a split-explicit, free-surface, topography-following-coordinate oceanic model," *Ocean Modelling*, vol. 9, pp. 347–404, 2005.

[18] A. Shchepetkin and J. McWilliams, "Quasi-monotone advection schemes based on explicit locally adaptive dissipation," *Monthly Weather Review*, vol. 126, pp. 1541–1580, 1998.

[19] Q. Vu, "JPL OurOcean portal." http://ourocean.jpl.nasa.gov/, 2008. viewed September 2010.

[20] Z. Li, Y. Chao, J. C. McWilliams, and K. Ide, "A three-dimensional variational data assimilation scheme for the regional ocean modeling system," *Journal of Atmospheric and Oceanic Technology*, vol. 25, pp. 2074–2090, 2008.

[21] E. E. Allmendinger, *Submersible Vehicle Systems Design*. The Society of Naval Architects and Marine Engineers, 1990.

[22] R. N. Smith, Y. Chao, P. P. Li, D. A. Caron, B. H. Jones, and G. S. Sukhatme, "Planning and implementing trajectories for autonomous underwater vehicles to track evolving ocean processes based on predictions from a regional ocean model," *International Journal of Robotics Research*, vol. 29, October 2010.

[23] R. N. Smith, J. Kelly, Y. Chao, B. H. Jones, and G. S. Sukhatme, "Towards improvement of autonomous glider navigation accuracy through the use of regional ocean models," in *Proceedings of the 29th International Conference on Offshore Mechanics and Arctic Engineering*, (Shanghai, China), June 2010.

[24] S. Boyd and L. Vandenberghe, *Convex Optimization*. Cambridge University Press, 2004.